Available online at www.sciencedirect.com
SCIENCE DIRECT®

Journal of the European Ceramic Society 24 (2004) 2399–2406
www.elsevier.com/locate/jeurceramsoc

Corrosion behavior of $MgO/CaZrO_3$ refractory matrix by clinker

Sara Serena*, M. Antonia Sainz, Angel Caballero

Instituto de Cerámica y Vidrio, C.S.I.C., Campus de Cantoblanco, 28049, Madrid, Spain

Received 10 March 2003; received in revised form 15 July 2003; accepted 19 July 2003

Abstract

The corrosion behavior of a $MgO/CaZrO_3$ refractory matrix by clinker of Portland cement is studied. The attack mechanism to substrates of 80% MgO and 20% $CaZrO_3$ (wt.%) obtained from dolomite and ZrO_2 mixtures and MgO and presintetized $CaZrO_3$ mixtures is established. The results are discussed in term of the phase equilibrium diagram $MgO–CaZrO_3–(CaO)_2SiO_2–(CaO)_3SiO_2$.

Keywords: Chrome-free refractories; Clinker; Corrosion; $MgO–CaZrO_3$; Refractories

1. Introduction

Magnesia–chromite bricks have been standard lining for the hot kiln zones since ~1940. Their properties, e.g. thermal conductivity, thermal shock resistance and thermal expansion, are mainly determined by the use of refractory grade chrome ores.[1]

The bonding of the bricks strongly influences the performance of a magnesia–chromite refractory lining. In the so-called direct bonded magnesia bricks, the grains are bonded tightly to the surrounding matrix. In general, the presence of alkalis in oxidizing atmosphere can degenerate the chrome–ore of magnesia–chromite bricks. The reaction is accompanied by the formation of toxic hexavalent chromates.[2,3] Recently, an increase in environmental concerns has pushed each company to strive for zero-emission status and/or to achieve the environmental isocertification. Nowadays, chrome-free bricks of magnesia–spinel type for the burning zone of rotary cement kilns have been developed.

For cement kilns refractories, MgO-oversaturated spinel are preferred as their eutectic of 2135 °C is much higher than the burning temperature of cement (1450 °C). Because of different thermal expansion coefficients between spinel and the magnesia matrix a microcrack system exists in the brick, which results in an increase of the elasticity. For this reason one of the methods for obtaining magnesia spinel bricks is the addition of alumina to a magnesia composition and the spinel is formed during the brick firing by an in-situ-reaction. Magnesia–spinel bricks are highly thermal shock resistant, not sensitive against reducing/oxidizing conditions, but are attacked by thermal overload. On the other hand, spinel forms low-melting phases with the result of a premature wear. To overcome this problem, latest developments are directed at an increasing use of $MgO–ZrO_2$ products in thermo-chemical stressed cement rotary kilns[4] because the zirconia has a higher resistance against attack by overheated cement clinker.[5]

Due to the formation of a so-called elastic direct bonding between MgO and $CaZrO_3$[1,6] and the high refractoriness of $CaZrO_3$ (2340 °C[7,8]), magnesia–calcium zirconate bricks are characterized by a high hot mechanical strength and excellent corrosion resistance against alkali, earth alkali oxides and basic slags. A deeper knowledge of the "behavior on service" and the wear mechanism are the main parameters to designs and/or optimize the $MgO/CaZrO_3$ materials in future developments.

Only Kozuka et al.[9,10] in Japan have studied the behavior of $MgO/CaZrO_3$ materials as a refractory material in rotary cement kilns. The postmortem analysis presented in these papers proved that the bricks showed superior corrosion resistance and coating adherence but peeled off easily in high stressed areas. There is no other works on the corrosion of $MgO/CaZrO_3$ material by

* Corresponding author.
E-mail address: serena@icv.csic.es (S. Serena).

0955-2219/$ - see front matter © 2003 Elsevier Ltd. All rights reserved.
doi:10.1016/j.jeurceramsoc.2003.07.007

cement, besides that mentioned, so that the attack mechanism involved is not actually established at all.

According with the tendency of recent years, the studies for improving the properties of the refractories are related to the optimization of the matrix by the careful design of the phase assemblage and the microstructure, so that the characterization of the microstructure of the materials is an important tool for the developement of the refractory. In this sense, the aim of this work is to study the behavior of $MgO/CaZrO_3$ matrixes, the most sensible fraction of the refractory material, to the attack by Portland cement at high temperatures.

The matrix proposed in the present study is constituted by 80% MgO and 20% $CaZrO_3$ (wt.%) obtained from mixtures of dolomite and ZrO_2, with addition of MgO in the proper stequiometry. A hand pressed piece of clinker of Portland cement (1.5 mm × 1.5 mm × 2 mm) is deposited on the matrix surface and heated al 1500 °C. Scanning electron microscopy (SEM) and microchemical analysis by energy dispersive X-ray analysis (EDS) of matrix-clinker interfacial reaction layers were performed on specimen cross sections.

2. Experimental procedure

The starting materials were high-purity powders of m–ZrO_2 (TZ-0, 99.9 wt.%, Tosoh Corp., Tokyo, Japan) with an average size, d_{50}, of <0.47 μm; high-purity dolomite ($MgCa(CO_3)_2$; Micro15, 99.9 wt.%, Prodomasa, Málaga, Spain) with d_{50} <4.87 μm; pure $CaCO_3$ (>99 wt.%, Fluka Chemical Corp., Ronkonkoma, NY) with d_{50} <4 μm; $CaZrO_3$ (>97 wt.%, ALFA Aesar, Johnson Mattey Company, Karlsruhe, Germany) with a bimodal size distribution centered in $d_{50}=0.27$ μm and $d_{50}=1.3$ μm; and MgO (>97 wt.%, MERCK, Damstadt, Germany) with d_{50} <35 μM.

Two samples with final compositions at 80% MgO and 20% $CaZrO_3$ were formulated. First from mixtures of m–ZrO_2, dolomite and MgO (80M-20CZ/D). The second one from MgO and commercial $CaZrO_3$ (80M-20CZ/C).

The processing route proposed was the following: the mixed powders of both compositions were first homogenized with isopropyl alcohol in an attrition miller for 2 h, dried at 60 °C followed by 60 μm sieving and isostatic pressing at 200 MPa to form green compact.

Dense substrates 80M-20CZ/C were obtained heating from room temperature at 5 °C/min up to 1600 °C for 2 h. The firing cycle for the substrate 80M-20CZ/D was the following: heating at 5 °C/min up to 900 °C, 1 h soaking time at 900 °C, heating at 5 °C/min up to 1600 °C, 2 h soaking time at 1600 °C. Dense cylinders were cut to obtain disc of 10 mm in diameter and 2 mm in height.

Hand-pressed pieces of 1.5 × 1.5 mm and 2 mm of clinker of cement (composition in Table 1) were deposited on the substrates surfaces. The couples clinker-substrate were thermally treated at 5 °C/min up to 1500 °C and maintained for 1 min or 3 h and then cooled at 10 °C/min.

Microstructural analysis and phase identification were done by optical microscopy and scanning electron microscopy (Zeiss DMS 950, Germany) with energy dispersive X-ray analyzer (SEM-EDS).

3. Results

Figs. 1 and 2 show a general view of the substrates 80M-20CZ/D and 80M-20CZ/C obtained by SEM. As observed, both substrates are composed by a matrix of MgO grains (dark phase) with $CaZrO_3$ (bright phase) generally located at grain boundaries and triple points. The porosity in both substrates was mainly intergranular. In the substrate 80M-20CZ/D (94% theoretical density), MgO grains around 2 μm and $CaZrO_3$ grains with a size between 0.5 and 1 μm were observed (Fig. 1). In the substrate 80M-20CZ/C (99% theoretical density), MgO grains between 5 and 15 μm were obtained. The $CaZrO_3$ grains with a size ~2 μm were

Table 1
Typical composition of the liquid phase, determined by EDS, in zone 2 (clinker near the interaction zone) and 3 (interaction zone) of the substrates reacted with clinker after the thermal treatment at 1500°/1 min[a]

		Liquid phase composition (wt.%)					
		CaO	Al_2O_3	Fe_2O_3	SiO_2	MgO	ZrO_2
Liquid clinker phase		50.1	23.7	19.5	3.9	2.8	–
80M-20CZ/D	Zone 2	47.0	19.8	20.5	5.4	2.9	4.4
	Zone 3	34.0	19.5	10.5	4.4	26.4	5.1
80M-20CZ/C	Zone 2	47.8	17.6	19.7	3.7	2.1	9.1
	Zone 3	48.6	15.6	23.5	2.7	3.6	5.9

[a] Composition of the liquid phase in the clinker is also included.

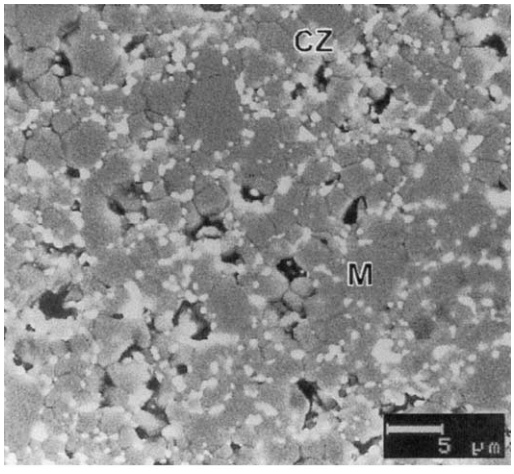

Fig. 1. Microstructure by SEM of the matrix 80M-20CZ/D, from dolomite and zirconia. M is MgO and CZ is $CaZrO_3$.

present forming agglomerates (Fig. 2). Note the differences between the grain size of both substrates.

Figs. 3 and 4 show the polished cross sections observed by optical microscopy of both substrates reacted with clinker at 1500 °C/1 min. Note that the pictures are actually a composition of two photographs. This is to show all the cross-section without missing any relevant feature, because of that, it was not possible to obtain all the field at a reasonable magnification. In both cases the hand pressed clinker appears separated from the substrates, although a layer of clinker seems to be adhered to the substrate surface.

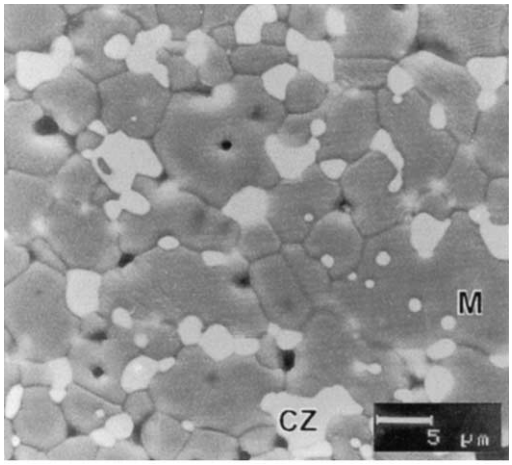

Fig. 2. Microstructure by SEM of the matrix 80M-20CZ/C, from magnesium oxide and presintetized calcium zirconate.

Figs. 5 and 6 show the polished cross sections observed by SEM of the same samples shown in Figs. 3 and 4 which confirmed the presence of a layer of adhered clinker on the surface of both substrates. The thickness of these mentioned layers were 10 μm on the substrate 80M-20CZ/D and 200 μm on the substrate 80M-20CZ/C.

The reaction between the clinker and the substrate produced different interaction areas. As it can be seen in Figs. 5a and 6a, the first zone (zone 1) corresponds to the original clinker, the second (zone 2) defined by the adhered layer of clinker which is on the interface and the third one (zone 3) is the reaction zone that occurs in the interface. SEM-EDS was used to determine the composition of the phases in the defined zones.

The EDS microanalysis performed in the clinker (zone 1) of the interaction zone, allowed us to establish that C_3S ($3CaO{\cdot}SiO_2$) and a liquid phase (average composition in wt.%: 50.1 CaO, 23.7 Al_2O_3, 19.5 Fe_2O_3, 3.9 SiO_2, 2.7 MgO) were the principal phases coexisting in the clinker.

For both substrates the layer of the clinker on the reaction zone (zone 2), again was constituted by C_3S as solid phase and a liquid phase whose composition for each substrate is shown in Table 1. Note that a light enrichment in ZrO_2 and no changes in MgO content were observed in the composition of the clinker-liquid compared with the composition in zone 1.

The thickness of the reaction zone (zone 3) was 60 μm in the 80M-20CZ/D substrate and 20 μm in the 80M-20CZ/C substrate. For both cases, a matrix of rounded

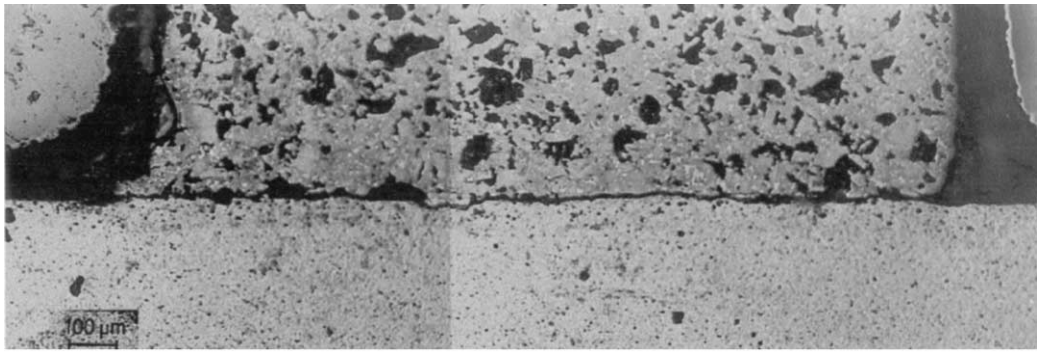

Fig. 3. Polished cross sections by optical microscopy of the sample clinker-80M-20CZ/D substrate at 1500 °C/ 1 min.

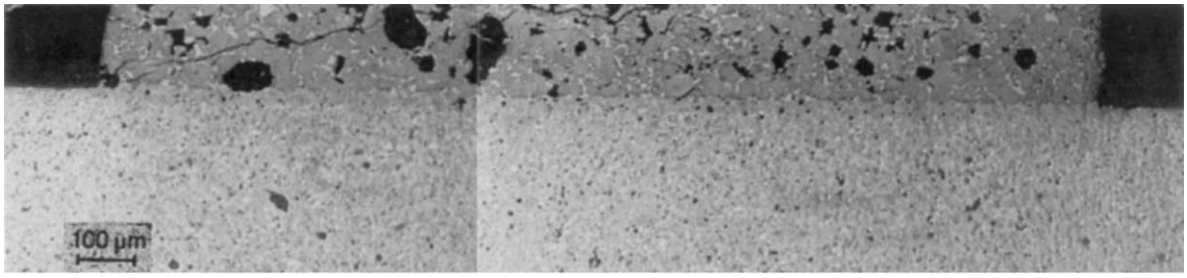

Fig. 4. Polished cross sections by optical microscopy of the sample clinker-80M-20CZ/C substrate at 1500 °C/ 1 min.

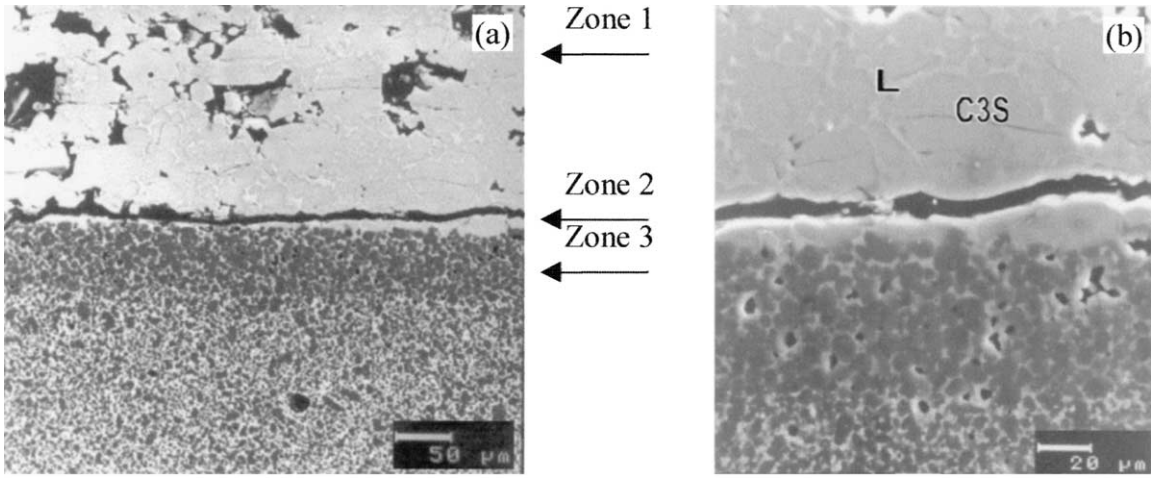

Fig. 5. Polished cross sections by SEM of the sample clinker-80M-20CZ/D, treated at 1500 °C/1 min. L is Liquid and C3S is $3CaO{\cdot}SiO_2$.

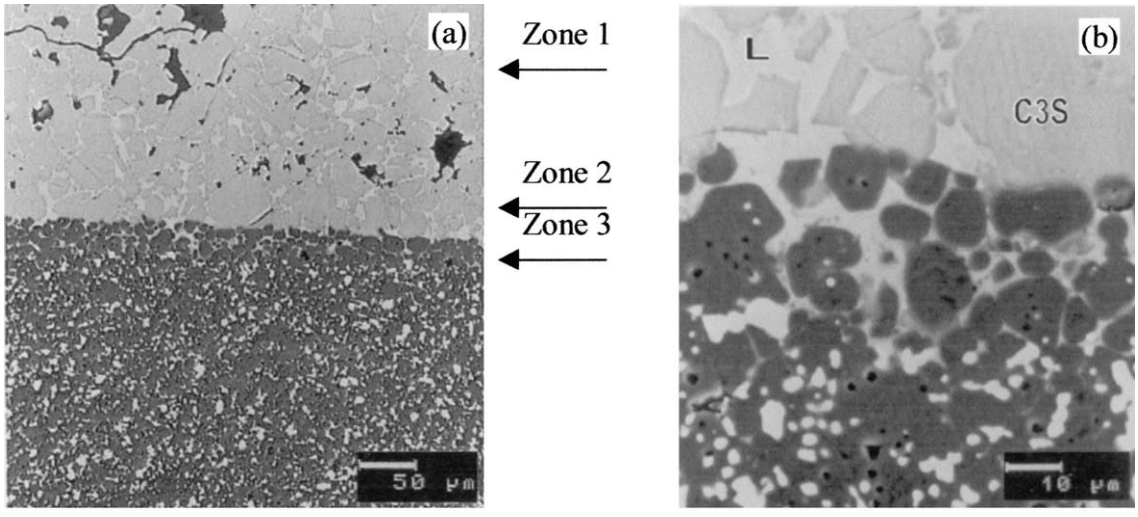

Fig. 6. Polished cross sections by SEM of the sample clinker-80M-2CZ/C, treated at 1500 °C/1 min. L is Liquid and C3S is $3CaO{\cdot}SiO_2$.

MgO grains, small C_3S crystals and a liquid phase (Figs. 5b and 6b) constituted this zone. The $CaZrO_3$ grains pre-existing in this zone were dissolved by the clinker-liquid phase and only small grains trapped in some MgO grains were observed in 80M-20CZ/C substrate. EDS microanalysis of the MgO grains revealed the presence of solid solutions of CaO (<2.5 wt.%) and Fe_2O_3 (<1.0 wt.%). The EDS microanalysis of the liquid phase in this zone for each substrate are collected in Table 1. The ZrO_2 content in the liquid phase in this area (zone 3) was very similar in both substrates and almost equal to that detected for the liquid phase in the zone 2. EDS microanalysis put in evidence the differences between the MgO content in the liquid phase in both substrates, 26.4 MgO wt.% in the 80M-20CZ/D and 3.6 MgO wt.% in the 80M-20CZ/C. Finally, it showed a significant decrease of iron oxide content in the liquid phase of the 80M-20CZ/D substrate, which is justified by the preferential diffusion of Fe_2O_3 into the substrate. This effect was clearly visible by the orange coloration observed under the reaction zone.

Under the interaction zone, substrates remain as their initial microstructure, and only a small quantity of liquid phase diffused throughout grain boundaries and pores. This effect was more evident in the 80M-20CZ/D sample.

Figs. 7a and 8a show SEM micrographs of the polished cross-section of clinker-substrates samples after firing at 1500 °C/3 h. In both samples, the clinker appears completely separated of substrates. At higher magnifications, no longitudinal or transversal cracks could be observed in the interfaces (Figs. 7b and 8b). In this experiment only two differential areas can be defined. The first area (zone 1) corresponds to the clinker and the second one (zone 2) is the reaction zone that occurs in the interface clinker–substrate.

The SEM-EDS analysis of the zone 1 confirmed that C_3S phase and liquid were the principal phases existing

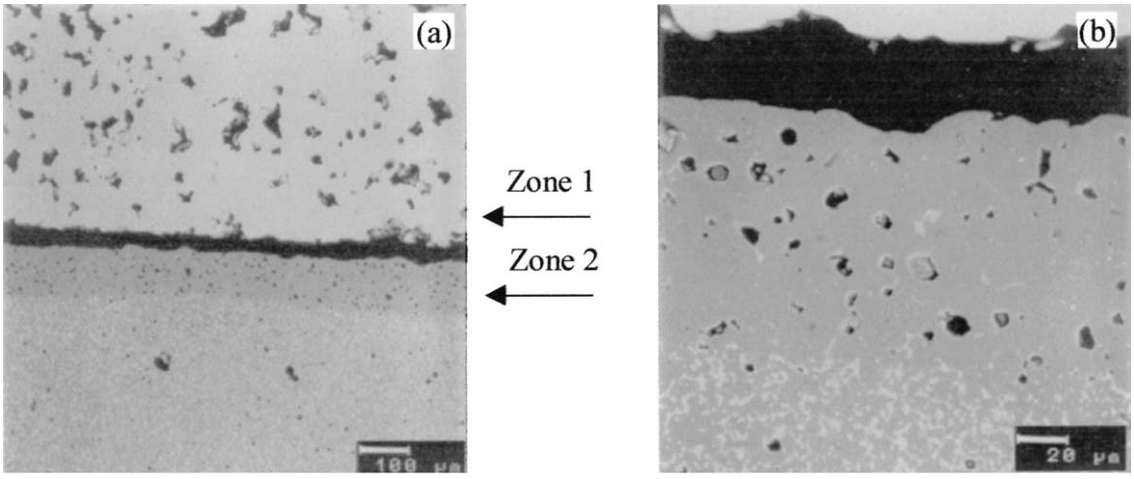

Fig. 7. Polished cross sections by SEM of the sample clinker-80M-20CZ/D, treated at 1500 °C/3 h.

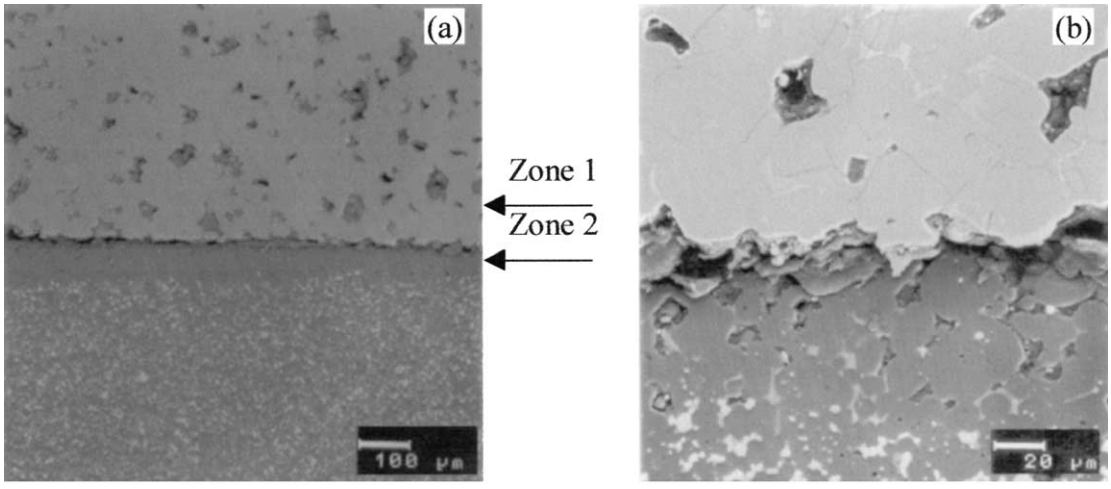

Fig. 8. Polished cross sections by SEM of the sample clinker-80M-20CZ/C, treated at 1500 °C/3 h.

in the clinker. The composition of the liquid clinker phase determined by EDS microanalysis in an area far enough into the interaction zone was totally similar to that previously determined in samples treated at 1500 °C/1min. The EDS microanalysis of the liquid phases nearest to the reaction zone (Table 2) were also similar to the liquid clinker composition for both substrates and only light enrichments in ZrO_2 contents were detected. This results clearly put in evidence the little interaction between the clinker and the substrates.

The thickness of the interaction zone (zone 2) was ~100 μm in the 80M-20CZ/D substrate (Fig. 7b) and ~50 μm in the 80M-20CZ/C substrate (Fig. 8b). For both substrates the interaction zone was constituted by sintered MgO grains and a small amount of liquid phase mainly trapped in triple points. Only in the substrate 80M-20CZ/C was it possible to observe $CaZrO_3$ grains entrapped in the MgO grains. Finally, the composition of the liquid phase, at triple points (Table 2), showed a similar tendency in both substrates with an increase in the CaO and SiO_2 content and a decrease in the Fe_2O_3 and Al_2O_3 content, reaching probably the corresponding composition in equilibrium with MgO. In fact, the chemical composition of the liquid in sample 80M-20CZ/D was very close to the liquid in equilibrium with MgO calculated from the CaO–SiO_2–MgO[11] system. Again, the preferential diffusion of Fe_2O_3 caused the coloration of the substrates, specially marked in 80M-20CZ/D.

As in the case of the thermal treatment for 1 min, below the interaction zone, the substrates remains as their initial microstructure, and only the presence of a small quantity of liquid phase diffused from the zone 3 throughout grain boundaries, and porosity was observed.

4. Discussion

The results obtained in the study of the attack mechanism to the substrates can be discussed in terms of the involved phase equilibrium diagrams.

Table 2
Typical composition of the liquid phase, determined by EDS, in zone 1 (clinker near the interaction zone) and 2 (interaction zone) of the substrates reacted with clinker after the thermal treatment at 1500 °C/3 h[a]

		Liquid phase composition (wt.%)					
		CaO	Al_2O_3	Fe_2O_3	SiO_2	MgO	ZrO_2
Liquid clinker phase		50.1	23.7	19.5	3.9	2.8	–
80M-20CZ/D	Zone 1	51.4	18.0	23.5	3.8	2.4	0.8
	Zone 2	59.8	–	2.2	19.5	17.6	0.9
80M-20CZ/C	Zone 1	52.8	16.7	22.8	4.0	2.1	1.6
	Zone 2	56.3	12.0	12.5	9.5	7.5	2.1

[a] Composition of the liquid phase in the clinker is also included.

The substrates, constituted by MgO and $CaZrO_3$, below the ternary system ZrO_2–CaO–MgO and the clinker, according their principal components can be analyzed considering the SiO_2–CaO–Al_2O_3–Fe_2O_3 system; however, taking into account that generally the only crystalline solid phases in the clinker are C_3S and C_2S, and that iron oxide and aluminum oxide present in the reaction zone are always located in the liquid phase, the reaction between the substrate and the clinker can be studied in terms of the MgO–CaO–ZrO_2–SiO_2 system and more specifically on the quaternary system MgO–$CaZrO_3$–C_3S–C_2S.

In despite of the invariant points of the subsystem MgO–$CaZrO_3$–C_3S–C_2S, reaching temperatures of 1700 and 1750 °C,[6] the presence of Al_2O_3 and Fe_2O_3 decrease the temperature of first liquid formation[12–14] up to ≈1200 °C, so that the following discussion on the basis of the proposed phase diagrams allows to interpret correctly the corrosion behavior of the samples.

The Fig. 9 shows a squematic representation of the primary crystallization volumes of MgO, $CaZrO_3$, C_2S and C_3S phases in the MgO–CaO–ZrO_2–SiO_2 system. This representation has been proposed from the bibliographic information.[6,12,13,15] The presence of the primary crystallization volume of CaO in the quaternary system is due to the incongruent fusion of C_3S phase.[6] In this system, the clinker composition is located inside the primary volume of C_3S phase while the substrates lie on the primary volume of the MgO phase. Then, the corrosion process on the substrates by the clinker takes place along the connection line between the clinker composition (CK), and the substrate composition (SB). The isothermal section at 1500 °C (Fig. 10) was estimated from previous studies.[6,12,13,15] The liquid composition, in equilibrium with the different phases was also determined for the samples treated 1500 °C/3h. All steps experimentally observed of the corrosion mechanism can be described in terms of the connection line CK-SB on the constructed isothermal section at 1500 °C.

At the initial step of the corrosion process (1500 °C/1 min), the liquid of clinker penetrates to the substrate through the open porosity and grain boundaries. This effect produces the decrease of the porosity in the reaction zone, the partial dissolution of MgO grains, the total dissolution of $CaZrO_3$ and the precipitation of C_3S in a limited region of the substrates surface (Figs. 5 and 6). The dissolution of $CaZrO_3$ grains cause the enrichment of the liquid phase in ZrO_2 (Table 1), increasing its viscosity. The phases present in the interface (Liquid + MgO + C_3S) are those expected from the proposed phase equilibrium diagram in the rich-clinker region (Fig. 10).

In the next step (1500 °C/3 h) the corrosion process progresses producing the total dissolution of the C_3S crystals in the interaction zone. The stable phases in this region are MgO and a liquid phase, again, that expected from the diagram (Fig. 10). An important grain growth of the MgO phase in the presence of a liquid phase happens, causing the formation of a layer of sintered MgO with liquid at triple points (Figs. 7 and 8). These liquid phases show low contents of Fe_2O_3 and Al_2O_3 (Table 2), due to the preferential diffusion of these oxides into the substrates. These oxides do not react to form other crystalline phases. As a consequence, the compositions of the remaining liquids are very close to the those in equilibrium with MgO in the system CaO–SiO_2–MgO.

Under the layer of sintered MgO, the substrates are constituted by MgO, $CaZrO_3$ and a small amount of liquid phase. This situation corresponds with that reflected by the proposed phase equilibrium diagram in the rich-substrate region (Fig. 10).

At this point, the corrosion process is ended, because the formed MgO layer is, at the same time, compatible and in equilibrium with the clinker and the substrate as can be deduced from Fig. 10.

The differences observed between both substrates are strongly related with their microstructural features. The higher porosity and fine grain size of the substrate 80M-20CZ/D enhances the penetration of liquid phase and the dissolution processes. These effects give rise to a faster corrosion in 80M-20CZ/D than in 80M-20CZ/C. As a consequence a larger size of the reaction zone in the 80M-20CZ/D substrate and a higher content of MgO in the liquid phase is observed at the initial steps of the corrosion (Table 1). The mentioned micro-

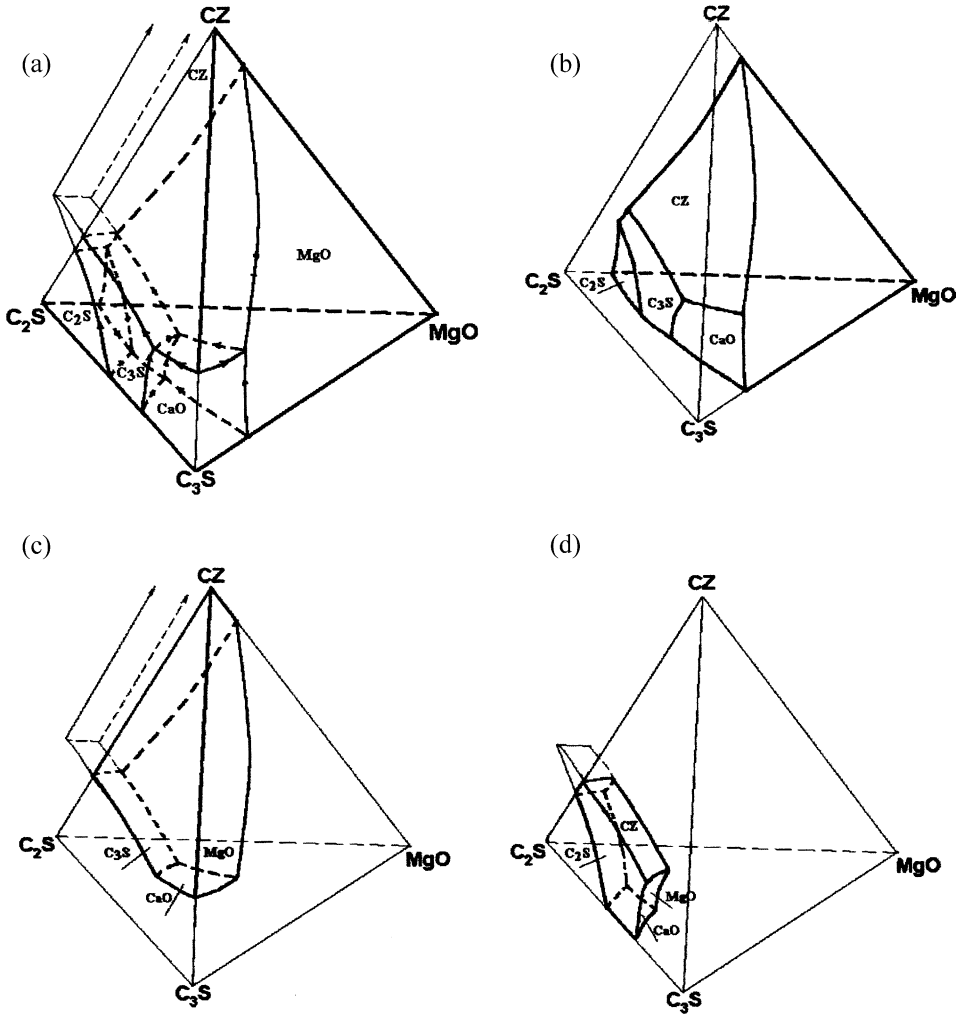

Fig. 9. Quarternary subsystem MgO–$CaZrO_3$–C_2S–C_3S (a). Primary crystallization volume of MgO (b), $CaZrO_3$ (CZ) (c) and C_3S (d).

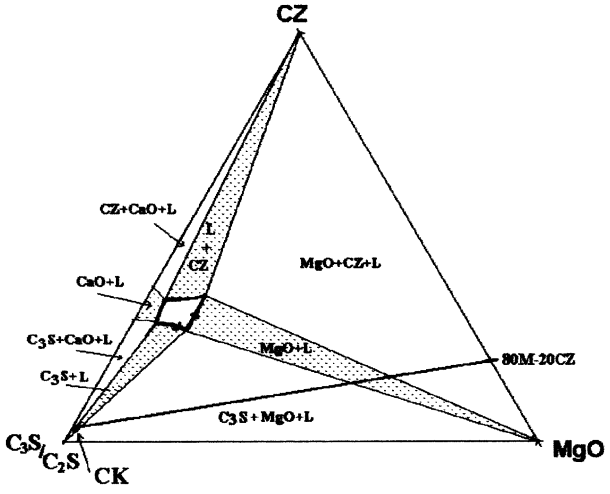

Fig. 10. Isothermal section of the isoplethal section MgO–$CaZrO_3$–C_nS of the subsystem MgO–$CaZrO_3$–C_3S–C_2S. C_nS correspond to the ratio C_3S/C_2S in a typical Portland cement clinker.

structural differences explain not only the different corrosion rate, but also the larger colored region observed into the 80M-20CZ/D substrate.

On the other hand, it is important to remark, that the attack does not cause the formation of cracks inside the substrate in any step of the process. However, a longitudinal crack is present in the samples after thermal treatments. These cracks are produced by the differences in the dilatation coefficients during the cooling of the samples. In the initial stages of the corrosion process the crack is located on the clinker–substrate interface, so that, a layer of clinker remains adhered to the surface of the substrates. By contrast, at the end of the corrosion process, the crack is located between the clinker and the substrate. This different behavior is related to the microstructure developed in the clinker–substrate interface during the attack. At the beginning of the corrosion process there is a continuos region where MgO, C_3S and a liquid phase coexist in the interface, so that the crack

produced by cooling appears in the clinker. At the end of the attack, the formation of the MgO sintered layer on the top of the substrates interrupts the continuity of the interface and propitiates the appearance of the crack along the clinker–substrate interface during cooling.

Finally, it is important to point out that the "in situ" formation of a clinker layer is very advantageous to prevent the corrosion of the refractory brick in work conditions.[9,10] From this work, it can be concluded that this clinker layer will be formed whenever microstructural continuity exists in the interface.

5. Conclusions

The corrosion behavior of 80% MgO and 20% $CaZrO_3$ (wt.%) materials by clinker of Portland cement has been established. Dense materials of $MgO/CaZrO_3$, obtained from both natural and synthetic raw materials, developed different microstructures. The microstructural features of the studied substrates determined the corrosion rate. In both cases, the corrosion process yield to the formation of a MgO sintered layer on the substrates that stopped the progress of the attack.

The corrosion behavior of the materials has been discussed in terms of the $MgO–CaZrO_3–C_3S–C_2S$ phase diagram. The experimental results are in good agreement with those deduced from the proposed diagram.

The studied matrix presented a clinker layer with good adherence that could prevent the corrosion of the refractory brick in work conditions, improving the corrosion resistance. The good corrosion behavior of the studied materials support their use as a matrix in magnesia chrome-free bricks for the burning zone of rotary cement kilns.

Acknowledgements

This work was supported by CYCIT, Spain, under project number MAT 2000-0941 and CAM, Madrid, Spain, under project number 07N/0038/2001.

References

1. Bartha, P. and Klischat, H. J., Present state of the refractory lining for cement kilns. *CN-Refractories*, 1999, **6**(3), 31–38.
2. Bray, D. J., Toxicity of chromium compounds formed in refractories. *Ceram. Bull.*, 1985, **64**(7), 1012–1016.
3. Driscoll, M. O., Price temper steel market promise. *Industrial Minerals*, 1994, **324**, 35–49.
4. Komatsu, H., Arai, M. and Ukawa, S., Current and future status of chrome-free bricks for rotary cement kilns. *Taikabutsu Overseas*, 1999, **19**(4), 3–9.
5. Bartha, P. and Klischat, H. J., Classification of magnesia bricks in rotary cement kilns according to specification and serviceability. *ZKG Intern.*, 1994, **47**(10), E277–E280.
6. De Aza, S., Richmond, C. and White, J., Compatibility Relationships of Periclase in the System $CaO–MgO–ZrO_2–SiO_2$. *Trans. and J. Brit. Ceram. Soc.*, 1974, **73**(4), 109–116.
7. Du, Y., Jin, Z. and Huang, P., Thermodynamical calculation of the zirconia–calcia system. *J. Am. Ceram. Soc.*, 1992, **75**(11), 3040–3048.
8. Du, Y., Jin, Z. and Huang, P., Calculation of the $ZrO_2–CaO–MgO$ system. *CALPHAD: Comput. Coupling Phase Diagrams Thermochem.*, 1992, **16**(3), 221–230.
9. Kozuka, H., Kaita, Y., Tuchiya, Y., Honda, T. and Ohta, S., New kind of chrome-free ($MgO–CaO–ZrO_2$) bricks for burning zone of rotary cement kiln. *Unitecr. 93, Sao Paulo, Brasil*, 1993, 1027–1037.
10. Kozuka, H., Kaita, Y., Tuchiya, Y., Honda, T. and Ohta, S., Further improvements of $MgO–CaO–ZrO_2$ bricks for burning zone of rotary cement kiln. *Unitecr. 95, Kyoto, Japan*, 1995, 256–263.
11. Kirschen, M. and De Capitani, C., Experimental determination and computation of the liquid miscibility gap in the system $CaO–MgO–SiO_2$-TiO_2. *Journal of Phase Equilibria*, 1999, **20**(6), 593–611.
12. Fabrichnaya, O. B. and Nerád, I., Thermodynamic properties of liquid phase in the $CaO·SiO_2–CaO·Al_2O_3·2SiO_2$-$2CaO·Al_2O_3·SiO_2$ system. *J. Eur. Ceram. Soc.*, 2000, **20**(4), 505–515.
13. Jak, E., Thermodynamic modelling of the system $Al_2O_3–SiO_2–CaO–FeO–Fe_2O_3$ to predict the flux requirements for coal ash slags. *Fuel and Energy Abstracts*, 1998, **39**(3), 231.
14. De Aza, A. H., Iglesias, E., Pena, P. and De Aza, S., The ternary system $Al_2O_3–MgO–CaO$. Part II. Phase relationships in the subsystem $Al_2O_3–MgAl_2O_4–CaAl_4O_7$. *J. Am. Ceram. Soc.*, 2000, **83**(4), 919–927.
15. Serena, S., Sainz, M. A., De Aza, S., Caballero, A., Thermodynamic assessment of the system $ZrO_2–CaO–MgO$ using new experimental results. Calculation of the isoplethal section $MgO·CaO–ZrO_2$,", (in preparation).